First-principles simulation of molecular dissociation–recombination equilibrium

Ilkka Kylänpää[a] and Tapio T. Rantala[b]
Department of Physics, Tampere University of Technology, P.O. Box 692, FI-33101 Tampere, Finland

(Received 25 May 2011; accepted 17 August 2011; published online 9 September 2011)

For the first time, the equilibrium composition of chemical dissociation–recombination reaction is simulated from first-principles, only. Furthermore, beyond the conventional *ab initio* Born–Oppenheimer quantum chemistry the effects from the thermal and quantum equilibrium dynamics of nuclei are consistently included, as well as, the nonadiabatic coupling between the electrons and the nuclei. This has been accomplished by the path integral Monte Carlo simulations for full NVT quantum statistics of the H_3^+ ion. The molecular total energy, partition function, free energy, entropy, and heat capacity are evaluated in a large temperature range: from below room temperature to temperatures relevant for planetary atmospheric physics. Temperature and density dependent reaction balance of the molecular ion and its fragments above 4000 K is presented, and also the density dependence of thermal ionization above 10 000 K is demonstrated. © *2011 American Institute of Physics*. [doi:10.1063/1.3633516]

I. INTRODUCTION

The H_3^+ molecular ion has been the subject of a number of theoretical and experimental studies since its first experimental detection.[1] Because of its rapid formation through the exothermic reaction ($\Delta E \approx -1.7$ eV),

$$H_2 + H_2^+ \rightarrow H_3^+ + H, \tag{1}$$

the H_3^+ ion is expected in any active environment containing molecular hydrogen,[2] and thus, it is encountered, e.g., in hydrogen plasma and in the atmosphere of giant planets.[3,4] This smallest polyatomic molecule dissociates to several fragments in a temperature and density dependent manner. It is a five-particle system, and therefore, small enough to allow related simulations based on first-principles, only.

In planetary atmospheric physics, importance of the H_3^+ ion lies in its capability to act as a cooling agent via infrared radiation.[5–7] The atmospheric models taking into account this cooling are commonly based on the high temperature molecular partition function of the H_3^+ ion.[2] Conventional evaluation of the partition function faces, however, a few challenges of which the first one is finding a good approximation to the infinite summation over all rovibrational quantum states with accurate enough energies.[2] This has usually been worked out with the calculations of a finite number of states from, e.g., a semi-empirical potential energy surface.[8]

The next challenge comes with the changing geometry of the H_3^+ ion at finite temperature. The rovibrational model needs to be extended for calculations of correct energetics for the emerging linear geometry of the weakly bound molecule.[5]

Finally, as pointed out above, at finite temperatures the molecule may also dissociate to its fragments, and in fact, the equilibrium reaction

$$\begin{aligned} H_3^+ &\leftrightarrow H_2 + p^+ \\ &\leftrightarrow H_2^+ + H \\ &\leftrightarrow 2H + p^+ \\ &\leftrightarrow H + 2p^+ + e^- \\ &\leftrightarrow 3p^+ + 2e^-, \end{aligned} \tag{2}$$

needs to be considered, the balance depending strongly on both the temperature and the density of H_3^+ ions.

This brings forth two questions, at the least. First, how relevant it is to consider the molecular energetics and related partition function at temperatures where the molecule has dissociated and appears in form of fragments of the equilibrium reaction, Eq. (2), only. Second, the balance of the equilibrium reaction may be strongly affected, not only by the density, but also by the environment including the neutralizing negative counterparts of the positive H_3^+. Thus, the thermal dissociation–recombination balance above dissociation temperature gives rise to problems, which have yet not been taken into account in this context.

To start with we first define the molecular partition function (and other molecular quantities) as the one of the system of particles that constitute the molecule. Thus, the low temperature limit gives us, in practice, the conventional textbook molecular partition function. However, this generalization allows us to extend the concept of molecular partition function (and the other molecular quantities) seamlessly to higher temperatures, where the molecule may dissociate and recombine in density and temperature dependent balance.

Similar definition of the molecule as a five-particle system allows us to carry out simulations of the full quantum statistics of the H_3^+ ion, now described by Eq. (2), at low densities and temperatures ranging from 160 K up to about 15 000 K using the path integral quantum Monte Carlo

[a]Electronic mail: ilkka.kylanpaa@tut.fi.
[b]Electronic mail: tapio.rantala@tut.fi.

(PIMC) method. PIMC is the method to meet the above challenges: we need not make any approximations or restrictions in the summing over states, geometries, or quantum effects in equilibrium dynamics. The finite temperature is inherent in the PIMC approach and the Coulomb many-body treatment of the particle–particle interactions is exact. The PIMC method is computationally expensive, but feasible for small enough systems.[9–14]

The conventional quantum chemical *ab initio* description of the H_3^+ ion emerges as the zero Kelvin extrapolate from the PIMC simulations as we have shown earlier.[15] There, we evaluated the differences between three models for the description of the nuclear dynamics: the Born–Oppenheimer approximation, nuclei in thermal motion and nuclei in both thermal and quantum dynamics. At low temperatures the necessity of the fully quantum mechanical approach for all five particles was established.

In Sec. II, we present the essential details of the Feynman path integral quantum statistical approach, numerical simulation method, and the model of the H_3^+ ion. In Sec. III, we present and analyze the energetics, partition function, and other thermodynamic functions of the system fitting to analytical forms where pertinent. In the last section the conclusions are given.

II. METHOD AND MODELS

According to the Feynman path integral formulation of the quantum statistical mechanics[16] the partition function of interacting distinguishable particles is given by the trace of the density matrix $\hat{\rho}(\beta) = e^{-\beta \hat{H}}$ as

$$Z = \mathrm{Tr}\hat{\rho}(\beta) = \int \mathrm{d}R_0 \mathrm{d}R_1 \ldots \mathrm{d}R_{M-1} \prod_{i=0}^{M-1} e^{-S(R_i, R_{i+1}; \tau)}, \tag{3}$$

where the action $S(R_i, R_{i+1}; \tau)$ is taken over the path $R_i \rightarrow R_{i+1}$ in imaginary time $\tau = \beta/M$, where $\beta = 1/k_\mathrm{B}T$ and M is called the Trotter number. The trace implies a closed path ($R_M = R_0$).

For simulation, we use the pair approximation in the action[9,17] for the Coulomb interaction of charges. This is exact in the limit $M \rightarrow \infty$, but chemical accuracy is reached with sufficiently large M, i.e., small enough τ. Sampling in the configuration space $\{R_i\}$ in NVT ensemble is carried out using the Metropolis algorithm[18] with bisection and displacement moves.[19] The total energy is calculated using the virial estimator,[20] which is proper for molecular energetics.

The error estimate in the PIMC scheme is commonly given in powers of the imaginary time-step τ.[9] Therefore, in order to systematically determine the thermal effects on the system we have carried out all the simulations with $\tau = 0.03 E_\mathrm{H}^{-1}$, where E_H denotes the unit of Hartree. Thus, the temperatures and the Trotter number M are related by $T = (k_\mathrm{B} M \tau)^{-1}$, where k_B is the Boltzmann constant.

In the following we mainly use the atomic units, where the lengths, energies, and masses are given in the units of Bohr radius (a_0), Hartree (E_H), and free electron mass (m_e), respectively. Thus, for the mass of the electrons we take $m_\mathrm{e} = 1$ and for the protons $m_\mathrm{p} = 1.836\,152\,672\,48 \times 10^3 m_\mathrm{e}$. Conversion of the units of energy is given by $E_\mathrm{H} = 219\,474.631\,370\,5\ \mathrm{cm}^{-1} \approx 27.2$ eV, and correspondingly, $k_\mathrm{B} = 3.166\,815\,2 \times 10^{-6} E_\mathrm{H}\,\mathrm{K}^{-1}$.

The statistical standard error of the mean (SEM) with 2 SEM limits is used as an error estimate for the evaluated observables.

For the NVT simulations, we place one H_3^+ ion, i.e., three protons and two electrons, into a cubic box and apply periodic boundary conditions and the minimum image principle. The simulations are performed in three different super cell (box) volumes: $(300a_0)^3$, $(100a_0)^3$, and $(50a_0)^3$. These correspond to the mass densities of $\sim 1.255 \times 10^{-6}\,\mathrm{g\,cm}^{-3}$, $\sim 3.388 \times 10^{-5}\,\mathrm{g\,cm}^{-3}$, and $\sim 2.710 \times 10^{-4}\,\mathrm{g\,cm}^{-3}$, respectively, which are relevant to H_3^+ ion containing atmospheres.[6] The density has no essential effect at low T, where dissociation rarely takes place. At higher T, however, the finite density gives rise to the molecular recombination balancing the more frequent dissociation.

It should be pointed out that application of the minimum image principle with only one molecular ion in the periodic super cell may give both rise to the finite-size effects and also disregard high density distribution effects, i.e., fragments of several ions in the simulation box. Thus, the lower the density the better we are able to minimize the finite-size effects, which in this work are negligible, if not absent. In principle, the zero density limit cannot be reached due to the finite T. To avoid all these high density distribution ambiguities we have defined our targets as molecular energetics, molecular partition function, and other related molecular quantities, at all temperatures and considered low densities. Therefore, in the following, we also exclude the trivial contribution from the center-of-mass thermal dynamics and energy $3/2 k_\mathrm{B} T$ to the molecular quantities.

We do not simulate the real-time quantum dynamics with our approach, but evaluate the quantum statistics of the thermal equilibrium from the imaginary time paths of particles. However, the energetics and other expectation values evaluated from the correct quantum statistics inherently include all contributions from the equilibrium thermal motion and quantum dynamics in translationally, vibrationally, and rotationally excited states.[16] With rising temperature, the thermal contribution takes over leading to the classical limit, whereas decrease towards zero Kelvin takes to the quantum limit, where only the zero point motion remains.[15]

The contribution to energetics from nuclear quantum dynamics, which was shown to be essential at low T, turns out to be negligible at higher temperatures. It is included, however, to be consistent with the low temperature results and our earlier study. Also, the distinguishable particle (boltzmannon) simulation was shown to be accurate for the nuclei due to the negligible overlap of nuclear wavefunctions and the two electrons in singlet state. Now, at higher temperatures both assumptions are still valid as the direct Franck–Condon transition energies of H_3^+ and H_2 to the lowest triplet state are still more than an order of magnitude larger than the thermal energy of these molecules in our simulations.[21–23] For the free fragments, the overlap of electronic wavefunctions is again

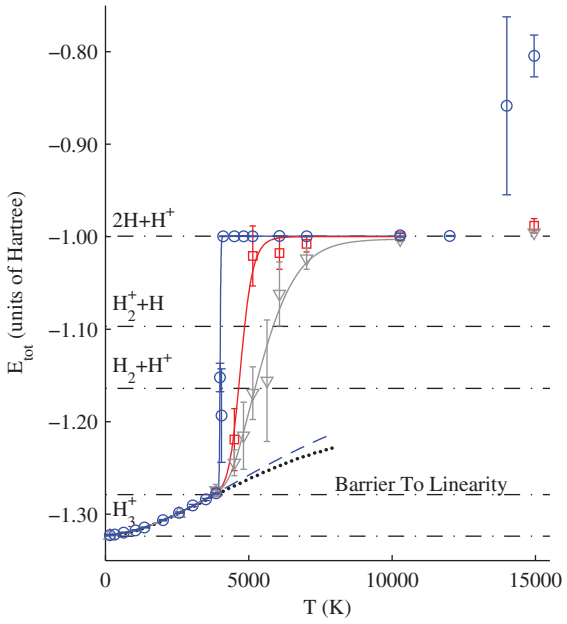

FIG. 1. NVT total energy of the H_3^+ molecular ion as a function of temperature at three different densities: blue circles ($\sim 1.255 \times 10^{-6}$ g cm^{-3}), red squares ($\sim 3.388 \times 10^{-5}$ g cm^{-3}), and gray triangles ($\sim 2.710 \times 10^{-4}$ g cm^{-3}). The blue dashed line is the energy fitted to Eq. (7). The black dots give the energy computed using the partition function fit given in Ref. 2. The horizontal dashed-dotted lines are the nonadiabatic zero Kelvin energies for the ion, its fragments and the barrier to linearity. The high temperature solid lines are mainly for guiding the eye, but used later for numerical evaluation of the partition function.

negligible and contributions from the weak overlapping configurations turns out to be vanishing.

For more details about the model and a discussion about the here neglected contribution from the exchange interaction, see Ref. 15.

III. RESULTS AND DISCUSSION

A. Overview of molecular energetics

In Fig. 1, the NVT total energy (canonical ensemble internal energy) of the H_3^+ ion and its fragments is shown as a function of temperature. The molecular energy does not include the center-of-mass translational kinetic energy $3/2k_BT$. The data from simulations are given as circles, squares, and triangles corresponding to the three densities. The PIMC data is also given in Tables I and II.

The solid lines at $T < 4000$ K are fitted to analytical model forms but at higher temperatures lines are only for guiding the eye. Our low temperature fit and analytical model, Eq. (8), is given as a blue dashed line and it is discussed in Secs. III B and III C in more detail. For comparison, the energies from the fitted partition function of Ref. 2 is shown as black dots. These two do not manifest dissociation, and therefore, are not relevant at "higher T."

The horizontal dashed-dotted lines show the zero Kelvin energies for the ion and its fragments in Eq. (2). One of these lines presents the energy for the "barrier to linearity," i.e., the minimum energy needed for the transformation to the linear molecular geometry on the zero Kelvin Born–Oppenheimer surface.

TABLE I. NVT energetics of the H_3^+ molecular ion at low temperatures—here the same data applies for all three densities. The energies are given in the units of Hartree (atomic units) and with 2 SEM error estimates. The energies from our low T fit (LTFIT) from Eq. (7) and those from the fit of Ref. 2 (NT) are also given as comparison. At 0 K, the best upper bound is given, see the footnote *c*.

$T(K)$	PIMC[a]	LTFIT[a]	NT fit[b]
0		−1.3231	(−1.32367)[c]
∼160.61	−1.3227(7)	−1.3227	−1.3232
∼321.22	−1.3221(6)	−1.3220	−1.3225
∼642.45	−1.3198(6)	−1.3202	−1.3209
∼1052.6	−1.3173(7)	−1.3171	−1.3179
∼1365.2	−1.3143(5)	−1.3141	−1.3148
∼2000.3	−1.3064(7)	−1.3065	−1.3070
∼2569.8	−1.2983(8)	−1.2984	−1.2989
∼3049.2	−1.2905(12)	−1.2909	−1.2917
∼3499.3	−1.2840(12)	−1.2835	−1.2847
∼3855.6	−1.2774(7)	−1.2774	−1.2792

[a]This work.
[b]Calculated from the fit given in Ref. 2.
[c]Para-H_3^+, see Refs. 23 and 25.

Within the considered molecular densities, $T \approx 4000$ K can be considered as apparent dissociation temperature. The energetics below 4000 K is so close to density independent that the differences between the three curves in Fig. 1 cannot be seen.

Above 4000 K, the density dependence is clearly seen as varying composition of fragments. In the range from 4000 to 10 000 K, the changing dissociation–recombination balance leads to distinctly different energetics, and above that, at our highest simulation temperatures the thermal ionization of hydrogen atoms starts contributing to the energy. However, it is worth pointing out that the temperature limits of these three ranges, i.e., about $0 - 4000$ K, about $4000 - 10\,000$ K, and above 10 000 K, are subject to changes with larger variation of densities.

TABLE II. PIMC NVT energetics of the H_3^+ molecular ion at high temperatures for the three densities (expressed as the number of molecular ions per volume), see Fig. 1. Notations are the same as in Table I.

$T(K)$	$(300a_0)^{-3}$	$(100a_0)^{-3}$	$(50a_0)^{-3}$
∼3999.2	−1.152(16)		
∼4050.0	−1.19(6)		
∼4100.4	−0.9995(4)		
∼4498.2	−0.9993(4)	−1.219(34)	−1.244(15)
∼4819.5	−0.9993(4)		−1.215(37)
∼5139.6	−0.9995(4)	−1.020(33)	−1.169(29)
∼5634.8			−1.156(66)
∼6070.3	−0.9991(4)	−1.018(18)	−1.062(35)
∼7017.2	−0.9995(4)	−1.008(9)	−1.024(12)
∼10279	−0.997(3)	−0.9995(8)	−1.003(3)
∼12016	−0.9993(6)		
∼13997	−0.86(10)		
∼14951	−0.805(23)	−0.988(8)	−0.9957(8)

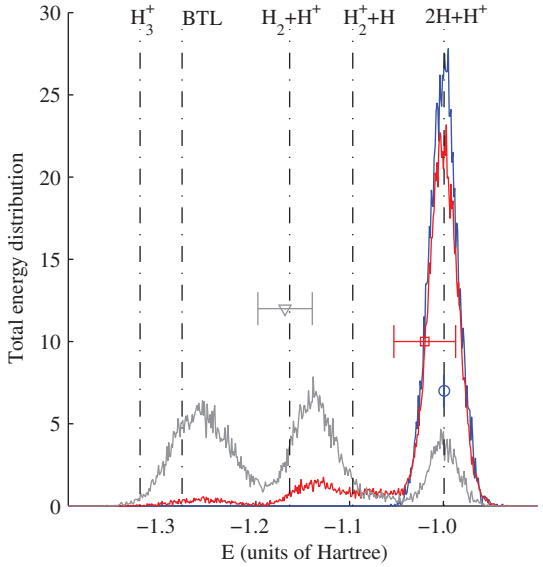

FIG. 2. Histogram of total energy sampling pinned in boxes of width $0.001\,E_{\mathrm{H}}$ from at least $(2 \times 10^4) \times 10^5$ Monte Carlo samples averaged over blocks of 10^5 samples. The energy expectation values are also given with 2 SEM error estimates. The temperature and the Trotter number are ∼5139.6 K and 2048, respectively. The histograms are normalized to unity for all three densities. Other notations are taken from Fig. 1.

Above 10 000 K, in our lowest density case the thermal ionization of H atoms is evident, see Fig. 1, but for our higher density cases some 15 000 K is needed to bring up first signs of ionization. Similar trend for the ionization is stated in Ref. 24, although the density is notably less than our lowest one.

Let us now consider the dissociation–recombination reaction chain, Eq. (2), and the contributing fragments to the quantum statistical NVT equilibrium trying to give an intuitive classical-like picture of the composition. With finite T, instead of zero, we have finite β, instead of infinite, that brings classical nature to the system the more, the higher the temperature. In other words, the partial decoherence in our five-particle quantum system increases with increasing temperature, that enables us to distinguish the fragments as separate molecules and atoms in thermal equilibrium. Based on this interpretation, we show the total energy distribution in Fig. 2 from sampling the imaginary time paths at about 5000 K with $M = 2048$ for all considered densities.

For our highest density (gray in Fig. 2), for example, we see three main peaks and by inspection of the energy distribution the first and the second can clearly be assigned to the rovibrationally excited H_3^+ and $H_2 + H^+$, respectively. As there are no rovibrational excitations available for $2H + H^+$, the third main peak average position is very close to $-1\,E_{\mathrm{H}}$. The fourth fragment, $H_2^+ + H$, can be identified as the small high-energy side shoulder of $H_2 + H^+$ peak. With the interpretation of the area under the peak as the abundance of the fragment in the equilibrium we find this contribution to be much smaller than that of the others, for which we can suggest following explanations. Probably due to loose binding of H_2^+ the distribution of its energetics is broad, and therefore, partly covered by the neighboring narrow peaks. Also, the larger entropy factor $-TS$ in free energy of the three particle system $2H+H^+$ increases its contribution. Lower densities make this effect even stronger as is distinctly seen in the Fig. 2.

It is important to note, however, that the above illustration is dependent on the block averaging procedure, see the caption of Fig. 2. Pinning the energy data of each and every sample, i.e., choosing block of size one sample, would broaden the peaks in Fig. 2. At the opposite limit, all samples in one block, would give the single mean energy or the ensemble average corresponding to the quantum statistical expectation value. From the highest density to the lowest, the expectation values are $-1.169(29)E_h$, $-1.020(33)E_h$, and $-0.9995(4)$, respectively, Figs. 1 and 2, where the statistical uncertainty decreases with increasing simulation length.

B. Molecular partition function

To compare with the other published approaches for the molecular partition function based on single molecule quantum chemistry we start from the lowest temperature range from 0 to ∼4000 K, where the molecule does not essentially dissociate, yet.

We present a low temperature H_3^+ molecular partition function as a first approximation for the modeling of low density H_3^+ ion containing atmospheres. Our aim is to find a simple analytical form, which can be accurately fitted to the NVT energies from our simulations.

The partition function in terms of the Helmholtz free energy F is written as

$$Z = e^{-\beta F}, \tag{4}$$

where $\beta = (k_{\mathrm{B}}T)^{-1}$, and the energy expectation value is straightforwardly derived from the partition function as

$$\langle E \rangle = -\frac{1}{Z}\frac{\partial Z}{\partial \beta}. \tag{5}$$

After solving the free energy from Eq. (4) as

$$F(T) = -k_{\mathrm{B}}T \ln Z(T), \tag{6}$$

we write $F(T) = -k_{\mathrm{B}}T f(T)$ and the energy expectation value may be written as

$$\langle E \rangle = k_{\mathrm{B}}T^2 \frac{\partial f(T)}{\partial T}. \tag{7}$$

We find that a well-behaving function fitting perfectly into our simulation data,

$$\langle E \rangle = k_{\mathrm{B}}T^2(ae^{-bT} + c) + de^{-\alpha/T}, \tag{8}$$

allows analytical integration of Eq. (7) for $f(T)$ or $\ln Z(T)$,

$$\ln Z(T) = -\frac{a}{b}e^{-bT} + cT + \frac{d}{k_{\mathrm{B}}\alpha}e^{-\alpha/T} + D. \tag{9}$$

Using the boundary condition for the molecular partition function with a nondegenerate ground state, $Z(0) = 1$ or $\ln Z(0) = 0$, we get $D = a/b$ in our model. Another choice, inclusion of the contributions from the ground state spin degeneracy factor and the zero-point rotations would give $Z(0) = \xi > 1$ and $D = a/b + \ln \xi$, and thus, shift the function $\ln Z$ by a constant, only. We have chosen the first and more conventional boundary value, $Z(0) = 1$.

The weighted least squares fit of the above energy function, Eq. (8), to our data for temperatures up to about 3900 K, see Table I, gives the parameters,

$$a = 0.00157426,$$
$$b = 0.000132273,$$
$$c = -6.15622 \times 10^{-6},$$
$$d = 0.00157430,$$
$$\alpha = 269.410, \text{ and}$$
$$D = a/b \approx 11.9016.$$

In the fit, in addition to the $(2\text{SEM})^{-2}$ weights, we force the first derivative of the energy with respect to the temperature to be monotonically increasing up to 3900 K. The fit extrapolates the 0 K energy to about $0.000\,549 E_{\text{H}}$ above that of the para-H_3^+, i.e., it gives an excellent match within the statistical error estimate.

In Fig. 3, the function $\ln Z(T)$ from Eq. (9) is shown in the range $0 < T < 4000$ K — the behavior of the model at higher T is illustrated by the dashed line. Above 4000 K, the three curves for different densities are obtained from those shown in Fig. 1 by numerical integration of Eq. (7) as

$$\ln Z(T) = \ln Z(T_1) + \int_{T_1}^{T} \frac{\langle E \rangle}{k_{\text{B}} T^2} \mathrm{d}T, \tag{10}$$

where $T_1 = 500$ K.

In Ref. 2, Neale and Tennyson (NT) have presented the partition function $\ln Z(T)$ based on a semi-empirical potential energy surface, see Fig. 3. The NT partition function has conventionally been used in atmospheric models. The overall shape is similar to the one of ours. However, the energy $\langle E \rangle$ evaluated from their fit tends to be systematically lower than ours, although roughly within our 2SEM error limits. Thus, the deviations are not visible in Fig. 1. The energy zero of the NT fit, black dots in Figs. 1 and 3, is the same as ours in this work, and thus, allows direct comparison in Fig. 1.

Also in Fig. 3, the difference due to the choice of the $J = 0$ state as the zero reference is illustrated by the NT partition function values, black pluses — the shape is notably affected at low T, only. As mentioned above, already, the zero reference of $\ln Z$ can be chosen differently.

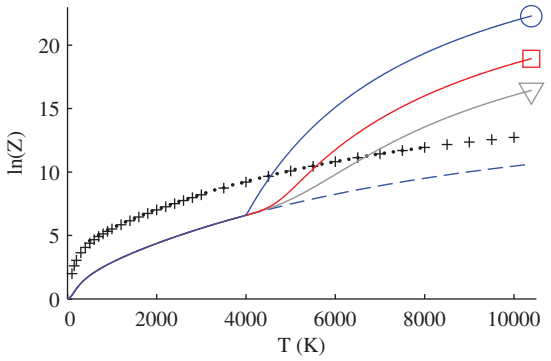

FIG. 3. The molecular NVT ensemble $\ln Z(T)$ from the energetics in Fig. 1 with the same notations. The blue solid line below 4000 K and its extrapolation (dashed line) are from Eq. (9), whereas the curves for three densities are from Eq. (10). The $\ln Z(T)$ data (black pluses) and the fit (black dots) of Ref. 2 are also shown. The black dots have the same zero energy as the partition function of this work (see text).

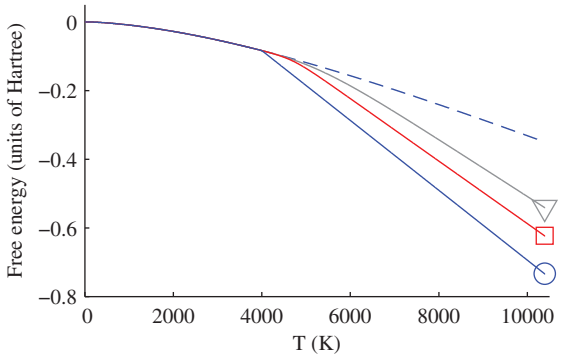

FIG. 4. Helmholtz free energy from Eq. (5) in the units of Hartree. Notations are the same as in Fig. 3.

Our low temperature partition function, Eq. (9), is close to complete. With the PIMC approach, we implicitly include all of the quantum states in the system with correct weight without any approximations. This partition function is the best one for the modeling of the low density H_3^+ ion containing atmospheres, at the moment. However, it is valid up to the dissociation temperature, only. As soon as the density dependence starts playing larger role, more complex models are needed. Such models can be fitted to our PIMC data given in Tables I and II.

C. Other thermodynamic functions

In Fig. 4, we show the Helmholtz free energy from combined Eqs. (6) and (9). As expected, lower density or larger volume per molecule lowers the free energy due to the increasing entropic factor. Dissociation and the consequent fragments help in filling both the space and phase space more uniformly or in less localized manner.

This kind of decreasing order is seen more clearly in the increasing entropy, shown in Fig. 5. The entropy has been evaluated from

$$S = \frac{U - F}{T}, \tag{11}$$

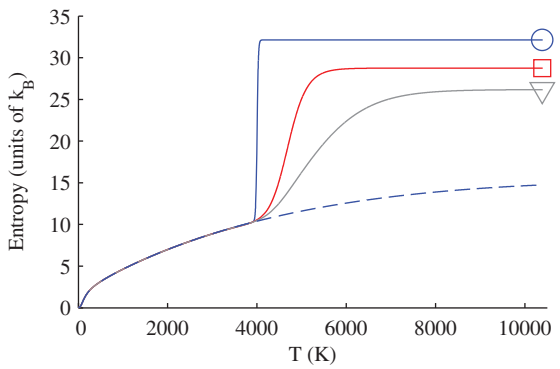

FIG. 5. Entropy from Eq. (11) in the units of k_{B}. Notations are the same as in Fig. 3.

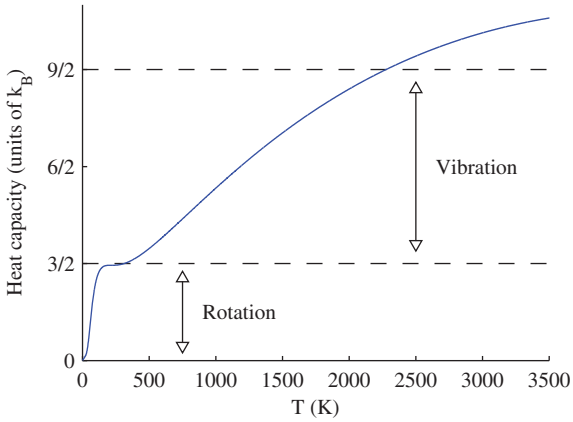

FIG. 6. Molecular heat capacity as a function of temperature calculated using the analytical model of this work. The values on the y-axis are given in units of the Boltzmann constant k_B.

where the internal energy is $U = \langle E \rangle - \langle E \rangle_{T=0}$. As expected, both the total energy (internal energy) and entropy reveal the dissociation taking place, similarly.

Finally, in Fig. 6, we present the molecular constant volume heat capacity

$$C_V = \frac{\partial \langle E \rangle}{\partial T}, \tag{12}$$

where $\langle E \rangle$ is taken from Eq. (8), which is valid below dissociation temperatures, only.

Considering the goodness of our functional form for $\langle E \rangle$, it is very convincing to see the plateau at about $3/2k_B$ corresponding to "saturation" of the contribution from the three rotational degrees of freedom. Thus, above 200 K the rotational degrees of freedom obey the classical equipartition principle of energy. It is the last term in the functional form of Eq. (8), that gives the flexibility for such detailed description of the energetics.

It should be emphasized that the plateau is not artificially constructed to appear at $3/2k_B$, except for a restriction given for the first derivative of the total energy to be increasing. Thus, the analytical model we present, Eq. (8), is found to be exceptionally successful at low temperatures, i.e., below dissociation temperature.

IV. CONCLUSIONS

We have evaluated the temperature dependent quantum statistics of the five-particle molecular ion H_3^+ at low densities far beyond its apparent dissociation temperature at about 4000 K. This is done with the PIMC method, which is basis set and trial wavefunction free approach and includes the Coulomb interactions exactly. Thus, we are able to extend the traditional *ab initio* quantum chemistry with full account of correlations to finite temperatures without approximations, also including the contributions from nuclear thermal and equilibrium quantum dynamics.

At higher temperatures, the temperature dependent mixed state description of the H_3^+ ion, the density dependent equilibrium dissociation–recombination balance, and the energetics have been evaluated for the first time. With the rising temperature the rovibrational excitations contribute to the energetics, as expected, whereas the electronic part remains in its ground state in the spirit of the Born–Oppenheimer approximation. At about 4000 K the fragments of the molecule, $H_2 + H^+$, $H_2^+ + H$, and $2H + H^+$, start contributing. Therefore, presence of the H_3^+ ion becomes less dominant and eventually negligible in high enough T.

We have also shown how the partial decoherence in the mixed state can be used for interpretation of the fragment composition of the equilibrium reaction. Furthermore, we have evaluated explicitly the related molecular partition function, free energy, entropy, and heat capacity, all as functions of temperature. An accurate analytical functional form for the internal energy is given below dissociation temperature. We consider all these as major additions to the earlier published studies of H_3^+, where the dissociation–recombination reaction has been neglected.

It is fair to admit, however, that PIMC is computationally heavy for good statistical accuracy and approximations are needed to solve the "Fermion sign problem" in cases where exchange interaction becomes essential. With H_3^+, however, we do not face the Fermion sign problem, as the proton wavefunctions do not overlap noteworthy and the two electrons can be assumed to form a singlet state, due to large singlet to triplet excitation energy.

ACKNOWLEDGMENTS

We thank the Academy of Finland for financial support, and we also thank the Finnish IT Center for Science (CSC) and Material Sciences National Grid Infrastructure (M-grid, akaatti) for computational resources.

[1] J. J. Thomson, Phil. Mag. **21**, 225 (1911).
[2] L. Neale and J. Tennyson, Astrophys. J. **454**, L169 (1995).
[3] M. B. Lystrup, S. Miller, N. D. Russo, J. R. J. Vervack, and T. Stallard, Astrophys. J. **677**, 790 (2008).
[4] T. T. Koskinen, A. D. Aylward, and S. Miller, Astrophys. J. **693**, 868 (2009).
[5] L. Neale, S. Miller, and J. Tennyson, Astrophys. J. **464**, 516 (1996).
[6] G. J. Harris, A. E. Lynas-Gray, S. Miller, and J. Tennyson, Astrophys. J. **600**, 1025 (2004).
[7] T. T. Koskinen, A. D. Aylward, C. G. A. Smith, and S. Miller, Astrophys. J. **661**, 515 (2007).
[8] B. M. Dinelli, O. L. Polyansky, and J. Tennyson, J. Chem. Phys. **103**, 10433 (1995).
[9] D. M. Ceperley, Rev. Mod. Phys. **67**, 279 (1995).
[10] M. Pierce and E. Manousakis, Phys. Rev. B **59**, 3802 (1999).
[11] Y. Kwon and K. B. Whaley, Phys. Rev. Lett. **83**, 4108(4) (1999).
[12] L. Knoll and D. Marx, Eur. Phys. J. D **10**, 353 (2000).
[13] J. E. Cuervo and P.-N. Roy, J. Chem. Phys. **125**, 124314 (2006).
[14] I. Kylänpää and T. T. Rantala, Phys. Rev. A **80**, 024504 (2009).
[15] I. Kylänpää and T. T. Rantala, J. Chem. Phys. **133**, 044312 (2010).
[16] R. P. Feynman, *Statistical Mechanics* (Perseus Books, Reading, MA, 1998).
[17] R. G. Storer, J. Math. Phys. **9**, 964 (1968).
[18] N. Metropolis, A. W. Rosenbluth, M. N. Rosenbluth, A. H. Teller, and E. Teller, J. Chem. Phys. **21**, 1087 (1953).
[19] C. Chakravarty, M. C. Gordillo, and D. M. Ceperley, J. Chem. Phys. **109**, 2123 (1998).
[20] M. F. Herman, E. J. Bruskin, and B. J. Berne, J. Chem. Phys. **76**, 5150 (1982).
[21] M. Misakian and J. C. Zorn, Phys. Rev. Lett. **27**, 174 (1971).

[22]Ch. Jungen, I. Dabrowski, G. Herzberg, and M. Vervloet, J. Chem. Phys. **93**, 2289 (1990).
[23]M. Pavanello and L. Adamowicz, J. Chem. Phys. **130**, 034104 (2009).
[24]T. T. Koskinen, R. V. Yelle, P. Lavvas, and N. K. Lewis, Astrophys. J **723**, 116 (2010).
[25]W. Kutzelnigg and R. Jaquet, Phil. Trans. R. Soc. A **364**, 2855 (2006).